SIAM J. SCI. COMPUT.
Vol. 24, No. 2, pp. 443–462

ON THE EFFICIENCY OF ADAPTIVE FINITE ELEMENT METHODS FOR ELLIPTIC PROBLEMS WITH DISCONTINUOUS COEFFICIENTS*

ZHIMING CHEN† AND SHIBIN DAI‡

Abstract. The successful implementation of adaptive finite element methods based on a posteriori error estimates depends on several ingredients: an a posteriori error indicator, a refinement/coarsening strategy, and the choice of various parameters. The objective of the paper is to examine the influence of these factors on the performance of adaptive finite element methods for a model problem: the linear elliptic equation with strongly discontinuous coefficients. We derive a new a posteriori error estimator which depends locally on the oscillations of the coefficients around singular points. Extensive numerical experiments are reported to support our theoretical results and to show the competitive behaviors of the proposed adaptive algorithm.

Key words. a posteriori error estimators, adaptive algorithm, performance

AMS subject classifications. 65N15, 65N30, 65N50

PII. S1064827501383713

1. Introduction.

A posteriori error estimates are computable quantities in terms of the discrete solution and data, which provide information for adaptive mesh refinement (and coarsening), error control, and equidistribution of the computational effort. Ever since the pioneering work of Babuška and Rheinboldt [3], the adaptive finite element methods based on a posteriori error estimates have become a central theme in scientific and engineering computations. We refer to the book of Verfürth [19] for an extensive review on residual type a posteriori estimators and the adaptive procedures and refer to Chen and Nochetto [6], Chen and Dai [5], Chen, Nochetto, and Schmidt [7], and Nochetto, Schmidt, and Verdi [16] for solving nonlinear partial differential equations arising from physical and industrial processes.

A successful implementation of an adaptive procedure includes several ingredients: an a posteriori error estimator, a refinement/coarsening strategy, and finally the determination of various parameters. The purpose of this paper is to explore the influence of these factors on the efficiency of adaptive finite element methods solving the second order elliptic equations with discontinuous coefficients

$$-\mathrm{div}(a(x)\nabla u) = f \quad \text{in } \Omega, \tag{1.1}$$

$$u = 0 \quad \text{on } \partial\Omega. \tag{1.2}$$

Here Ω is a polyhedral domain in $\mathbf{R}^d (d = 2, 3)$, the source function f is assumed to be in $L^2(\Omega)$, and the coefficient $a(x)$ is positive and piecewise constant. The extension of the results in the paper to the more general case when $a(x)$ is a piecewise constant positive definite symmetric matrix is straightforward. The problem (1.1)–(1.2) models a large variety of practical processes: steady state heat conduction in

*Received by the editors January 18, 2001; accepted for publication (in revised form) February 5, 2002; published electronically September 10, 2002.

http://www.siam.org/journals/sisc/24-2/38371.html

†LSEC, Institute of Computational Mathematics, Academy of Mathematics and System Sciences, Chinese Academy of Sciences, P.O. Box 2719, Beijing 100080, China (zmchen@lsec.cc.ac.cn). The research of this author was partially supported by China NSF grant 10025102 and China National Key Project "Large Scale Scientific Computation Research " (G1999032802).

‡Department of Mathematics, University of Maryland, College Park, MD 20742 (sdai@math.umd.edu).

composite materials, multiphase flow through heterogeneous porous media (Aziz and Settari [1]), or several layers of fluids with different viscosities depending weakly on the depth (Lewandowski [13]).

Let $\mathcal{M}_H$ be a regular triangulation of the domain Ω such that $a(x)$ is constant on each element $K \in \mathcal{M}_H$, and let $\mathcal{B}_H$ be the collection of all interelement sides of $\mathcal{M}_H$. Denote by u_H the piecewise linear conforming finite element solution over $\mathcal{M}_H$. For any interelement side $e \in \mathcal{B}_H$, let Ω_e be the collection of two elements sharing e and define the local error indicator η_e as

$$\eta_e^2 := \sum_{K\in\Omega_e} \| H_K f \|^2_{L^2(K)} + \| H_e^{1/2} J_e \|^2_{L^2(e)}, \tag{1.3}$$

where $H_K := \mathrm{diam}(K)$, $H_e := \mathrm{diam}(e)$, and $J_e := [\![a\nabla u_H]\!]_e \cdot \nu$ stands for the jump of flux across side e which is independent of the orientation of the unit normal ν to e. The following a posteriori error estimate is well known (see Babuška and Miller [2], Verfürth [19]):

$$\| u - u_H \|^2_{H^1(\Omega)} \le C \sum_{e\in\mathcal{B}_H} \eta_e^2. \tag{1.4}$$

The constant C in (1.4) depends on the coefficient $a(x)$; more precisely, it is proportional to $\max_{x\in\Omega} a(x)/\min_{x\in\Omega} a(x)$. This poor dependence on the coefficient $a(x)$ is rather inaccurate when $a(x)$ has large variations. In a recent paper [4], by working on the energy norm $|\!|\!| v |\!|\!|_\Omega = \| a^{1/2}\nabla v \|_{L^2(\Omega)}$, Bernardi and Verfürth derived the following a posteriori error estimate:

$$|\!|\!| u - u_H |\!|\!|^2_\Omega \le C \sum_{e\in\mathcal{B}_H} \eta_e^2, \tag{1.5}$$

where the local error indicator η_e is given by

$$\eta_e^2 := \sum_{K\in\Omega_e} \| H_K a_K^{-1/2} f \|^2_{L^2(K)} + \| H_e^{1/2} a_e^{-1/2} J_e \|^2_{L^2(e)}. \tag{1.6}$$

Here a_K is the constant value of $a(x)$ on $K \in \mathcal{M}_H$ and $a_e = \max_{K\in\Omega_e}(a_K)$. Let the domain Ω be split into disjoint open subdomains $\Omega_l, 1 \le l \le L$, such that $a(x)$ is constant on each Ω_l. The constant C in (1.5) can be made independent of the ratio $\max_{x\in\Omega} a(x)/\min_{x\in\Omega} a(x)$ under the assumption that for any two different subdomains $\bar\Omega_l$ and $\bar\Omega_k$ sharing at least one point, there is a connected path passing from $\bar\Omega_l$ to $\bar\Omega_k$ through adjacent subdomains such that the function $a(x)$ is monotone along this path (Hypothesis 2.7 in [4]). This result was extended to the quasi-monotone coefficients in Petzoldt [17]. The condition of quasi-monotone coefficients, however, rules out some interesting physical cases like the checkerboard discontinuous coefficients. The first objective of the paper is to propose a new a posteriori estimate and compare its performance to the above estimates (1.3) and (1.6) through numerical experiments.

For any node x, ω_x is referred to as the union of all elements sharing the common vertex x. Roughly speaking, the distribution of coefficients around a certain interior node x is quasi-monotone if the trace of $a(x)$ on a small sphere $B \subset \omega_x$ around x has only one local maximum. A local maximum is attained on $B \cap K_i$, $K_i \in \mathcal{M}_H$, if $a_{K_i} > a_{K_j}$ for all elements K_j in ω_x sharing one common side with K_i. If x is a boundary

node, then it is required for the quasi-monotone condition that each local maximum is adjacent to the boundary $\partial\Omega$. The precise definition of the quasi-monotone condition will be recalled in section 2. In this paper, the nodes with respect to which the quasi-monotone condition for the distribution of coefficients is violated will be called singular nodes. For any $K \in \mathcal{M}_H$, denote by $\omega_K := \cup\{K' \in \mathcal{M}_H : \bar{K} \cap \bar{K}' \neq \emptyset\}$. If K has one singular node, we set $\Lambda_K := \max_{K' \subset \omega_K}(a_K/a_{K'})$; otherwise, we set $\Lambda_K = 1$. We prove the following a posteriori error estimate for the elliptic problem (1.1)–(1.2):

$$\|\!|u - u_H|\!\|_\Omega^2 \leq C_1 \sum_{e \in \mathcal{B}_H} \eta_e^2, \tag{1.7}$$

where the constant C_1 depends only on the minimum angle of the triangulation $\mathcal{M}_H$, and the local error indicator η_e is given by

$$\eta_e^2 := \sum_{K \in \Omega_e} \Lambda_K \| H_K a_K^{-1/2} f \|_{L^2(K)}^2 + \Lambda_e \| H_e^{1/2} a_e^{-1/2} J_e \|_{L^2(e)}^2, \tag{1.8}$$

where $\Lambda_e = \max_{K \in \Omega_e} \Lambda_K$. Note that Λ_K is equal to one in the elements away from the singular nodes and active only around the singular nodes. This is the major improvement of our new local error estimator.

Based on the local error indicator, the usual adaptive algorithm solving the elliptic problem (1.1)–(1.2) reads as follows:

$$\text{Solve} \quad \rightarrow \quad \text{Estimate} \quad \rightarrow \quad \text{Refine/Coarsen}. \tag{1.9}$$

The important convergence property, which guarantees the iterative loop terminates in finite steps starting from an initial coarse mesh, is proved in Dörfler [9] and Morin, Nochetto, and Siebert [14]. The key point in the convergence analysis is the appropriate designing of refinement strategy. In this paper, we will use the refinement strategy proposed in [14] which improves the guaranteed error reduction strategy by [9]. This strategy depends only on two parameters $\theta, \hat{\theta}$; we will show that the choice of these two parameters also affects the efficiency of the adaptive algorithm through extensive numerical testings.

The final issue in the implementation of the adaptive algorithm (1.9) is the stopping criterion. The usual stopping criterion terminates the adaptive iteration (1.9) if the a posteriori error estimate satisfies $\sum_{e \in \mathcal{B}_H} \eta_e^2 \leq \varepsilon$ for some given tolerance $\varepsilon > 0$. This criterion, however, has the difficulty of the unknown constant C_1 in the upper bound of the a posteriori error analysis. Let $\mathcal{M}_k$ be the finite element mesh produced by the algorithm (1.9) in the kth iteration, u_k the corresponding finite element solution, and $\eta_k^2 = \sum_{e \in \mathcal{B}_k} \eta_e^2$ the a posteriori error estimate at the kth iteration. The quantity η_k/η_0 which measures the reduction rate of the a posteriori error estimates provides some information of the relative error $\|\!|u - u_k|\!\|_\Omega / \|\!|u - u_0|\!\|_\Omega$. Thus another possible stopping criterion is to terminate the adaptive algorithm (1.9) if $\eta_k/\eta_0 \leq \varepsilon$ for some given tolerance $\varepsilon > 0$.

The layout of the paper is as follows. In section 2 we prove the a posteriori estimate. In section 3 we modify the method in [14] to prove the convergence of the adaptive algorithm (1.9) based on the new a posteriori error estimator. In particular, we will show that the reduction rate of the adaptive algorithm depends on the factor $\max_{K \in \mathcal{M}_H} \Lambda_K$ and this dependence *cannot* be removed by constructing a counterexample. The numerical experiments in section 4 also confirm this dependence. In section 4 we present careful numerical experiments for a two-dimensional example to

test the performance of the new error estimator, to explore the dependence of the algorithm on the parameter θ, and to document the dependence of the reduction rate of the algorithm on the factor $\max_{K\in\mathcal{M}_H}\Lambda_K$ which reflects the degree of singularity of the underlying problem. In particular, we show that for the proposed adaptive method, the meshes and the associated numerical complexity are quasi-optimal: $\|\!|u-u_k|\!\|_\Omega = C\mathrm{DOFs}(k)^{-1/2}$ and $\|u-u_k\|_{L^\infty(\Omega)} = C\mathrm{DOFs}(k)^{-1}$ are valid asymptotically, where $\mathrm{DOFs}(k)$ is the number of degrees of freedom of the mesh $\mathcal{M}_k$.

2. A posteriori error analysis. We begin with introducing some notation. For any open set $G\subset\mathbf{R}^d$, we denote by $H^1(G)$ the standard Sobolev space of functions in $L^2(G)$ whose first derivatives are also in $L^2(G)$. The coefficient $a(x)$ is assumed to be piecewise constant and positive. Thus the seminorm $|\!|\!|\cdot|\!|\!|_G$ defined by $|\!|\!|v|\!|\!|_G^2 = (a\nabla v,\nabla v)_G$ is equivalent to the $H_0^1(\Omega)$ norm when $G=\Omega$. Here $(\cdot,\cdot)_G$ stands for the $L^2(G)$ inner product, and we will write $(\cdot,\cdot)=(\cdot,\cdot)_\Omega$. For any $f\in L^2(\Omega)$, the weak formulation of the problem (1.1)–(1.2) reads as follows:

$$u\in H_0^1(\Omega): \quad (a\nabla u,\nabla v)=(f,v) \quad \forall v\in H_0^1(\Omega). \tag{2.1}$$

Let $\mathcal{M}_H$ be a regular triangulation over Ω such that $a(x)$ is constant on each element K, and let $\mathcal{B}_H$ be the collection of all interelement sides of $\mathcal{M}_H$. Let V_H be the space of conforming linear finite element space over $\mathcal{M}_H$, and $V_0^H = V^H\cap H_0^1(\Omega)$. Let $u_H\in V_0^H$ be the solution of the discrete problem

$$u_H\in V_0^H: \quad (a\nabla u_H,\nabla v_H)=(f,v_H) \quad \forall v_H\in V_0^H. \tag{2.2}$$

We follow Petzoldt [17] to introduce the notation of the quasi-monotone condition of the distribution of coefficients (see also Dryja, Sarkis, and Widlund [10]). For each node x, let ω_x be the union of all elements K sharing x as the common node, and let C_x be all elements $K\subset\omega_x$ where the coefficients a_K achieve the maximum in ω_x. The distribution of coefficients $a_K, K\subset\omega_x$, will be called quasi-monotone with respect to x if the following conditions are fulfilled: For each element $K\subset\omega_x$ there exists a Lipschitz set $K_{x,qm}$ with $K\cup C_x\subset K_{x,qm}\subset\omega_x$ such that

$$a_K\le a_{K'} \quad \forall K'\subset K_{x,qm}, \quad K'\in\mathcal{M}_H.$$

If x is a boundary node, it is additionally required that $\mathrm{meas}_{d-1}(\partial K_{x,qm}\cap\partial\Omega)>0$. The nodes with respect to which the quasi-monotone condition is violated are called singular nodes. For further information about the quasi-monotone condition we refer to [10], [17], and [18].

For any $K\in\mathcal{M}_H$, H_K stands for its diameter. For any $e\in\mathcal{B}_H$, denote by H_e its diameter and by Ω_e the collection of two elements sharing the side e. For any $K\in\mathcal{M}_H$ and $e\in\mathcal{B}_H$, let

$$\omega_K=\cup\{K'\in\mathcal{M}_H : \bar K'\cap\bar K\neq\emptyset\}, \qquad \omega_e=\cup\{K'\in\mathcal{M}_H : \bar K'\cap\bar e\neq\emptyset\}.$$

The following quantity will play an important role in the subsequent analysis:

$$\Lambda_K := \begin{cases} \max\limits_{K'\in\omega_K}\left(\dfrac{a_K}{a_{K'}}\right) & \text{if } K \text{ has one singular node,}\\ 1 & \text{otherwise.}\end{cases} \tag{2.3}$$

Let η_e be the local error indicator associated with $e\in\mathcal{B}_H$ defined as

$$\eta_e^2=\sum_{K\in\Omega_e}\Lambda_K|\!|\!| H_K a_K^{-1/2} f|\!|\!|_{L^2(K)}^2+\Lambda_e|\!|\!| H_e^{1/2}a_e^{-1/2}J_e|\!|\!|_{L^2(e)}^2, \tag{2.4}$$

where $\Lambda_e = \max_{K\in\Omega_e} \Lambda_K$. The following upper bound improves the result in [2], [4], and [17].

THEOREM 2.1. *There exists a constant $C_1 > 0$ depending only on the minimum angle of $\mathcal{M}_H$ such that*

$$\|\!|u - u_H|\!\|_\Omega^2 \le C_1 \sum_{e\in\mathcal{B}_H} \eta_e^2. \tag{2.5}$$

Proof. The proof follows the argument in standard a posteriori error analysis and makes use of the robust interpolant in [10] and [17] $r_H : H_0^1(\Omega) \to V_0^H$ which satisfies the following two estimates:

$$a_K^{1/2} \| \phi - r_H\phi \|_{L^2(K)} \le C\Lambda_K^{1/2} H_K \|\!|\phi|\!\|_{\omega_K} \quad \forall \phi \in H_0^1(\Omega),\ \forall K \in \mathcal{M}_H, \tag{2.6}$$

$$a_e^{1/2} \| \phi - r_H\phi \|_{L^2(e)} \le C\Lambda_e^{1/2} H_e^{1/2} \|\!|\phi|\!\|_{\omega_e} \quad \forall \phi \in H_0^1(\Omega),\ \forall e \in \mathcal{B}_H. \tag{2.7}$$

Recall that $\Lambda_K = 1$ for elements away from the singular nodes. Subtracting (2.2) from (2.1) and integrating by parts yield

$$(a\nabla(u - u_H), \nabla\phi) = \sum_{K\in\mathcal{M}_H} (f, \phi - r_H\phi)_K + \sum_{e\in\mathcal{B}_H} \int_e J_e(\phi - r_H\phi) ds \tag{2.8}$$

for all $\phi \in H_0^1(\Omega)$. Using (2.6) we have

$$\begin{aligned}(f, \phi - r_H\phi)_K &\le \| f \|_{L^2(K)} \| \phi - r_H\phi \|_{L^2(K)} \\ &\le C\Lambda_K^{1/2} \| H_K a_K^{-1/2} f \|_{L^2(K)} \|\!|\phi|\!\|_{\omega_K}.\end{aligned}$$

Summing up over $K \in \mathcal{M}_H$ and making use of the regularity assumption of the mesh, we obtain

$$\sum_{K\in\mathcal{M}_H} (f, \phi - r_H\phi)_K \le C \left(\sum_{K\in\mathcal{M}_H} \Lambda_K \| H_K a_K^{-1/2} f \|_{L^2(K)}^2 \right)^{1/2} \|\!|\phi|\!\|_\Omega.$$

Similarly, using (2.7) we can get

$$\sum_{e\in\mathcal{B}_H} \int_e J_e(\phi - r_H\phi) ds \le C \left(\sum_{e\in\mathcal{B}_H} \Lambda_e \| H_e^{1/2} a_e^{-1/2} J_e \|_{L^2(e)}^2 \right)^{1/2} \|\!|\phi|\!\|_\Omega.$$

This completes the proof upon taking $\phi = u - u_H$ in (2.8). ∎

The following local lower bound can be proved by the method of Verfürth [19].

THEOREM 2.2. *There exist two constants $C_2, C_3 > 0$ depending only on the minimum angle of $\mathcal{M}_H$ such that, for any $e \in \mathcal{B}_H$,*

$$\eta_e^2 \le C_2\Lambda_e \sum_{K\in\Omega_e} \|\!|u - u_H|\!\|_K^2 + C_3\Lambda_e \sum_{K\in\Omega_e} \| H_K a_K^{-1/2} (f - f_K) \|_{L^2(K)}^2,$$

where $f_K = \frac{1}{|K|} \int_K f dx$, $\Lambda_e = \max_{K\in\Omega_e}(\Lambda_K)$.

Remark 2.1. The appearance of the factor Λ_e is somewhat annoying, but the counterexample in the appendix strongly suggests that this factor cannot be removed in general.

Remark 2.2. In practical applications there might be a large number of different singularities. In this situation, it might be difficult to distinguish all the singular nodes in the program at each adaptive iteration. Then the following enlarged a posteriori error estimator could be useful:

$$\bar{\eta}_e^2 = \sum_{K\in\Omega_e} \bar{\Lambda}_K \| H_K a_K^{-1/2} f \|_{L^2(K)}^2 + \bar{\Lambda}_e \| H_e^{1/2} a_e^{-1/2} J_e \|_{L^2(e)}^2,$$

where $\bar{\Lambda}_K = \max_{K'\in\omega_K}(a_K/a_{K'})$ and $\bar{\Lambda}_e = \max_{K\in\Omega_e} \bar{\Lambda}_K$. Note that $\bar{\Lambda}_K$ is equal to one on the elements away from the places where the coefficient jumps.

3. The adaptive algorithm and its convergence. In this section we show the convergence of the adaptive loop (1.9) based on the a posteriori error estimator in section 2 and the refinement strategy in [14]. The analysis depends largely on the methods in [14], and so we will concentrate only on the differences. The main objective here is to track down the dependence of error reduction rate on the variation of the coefficients, which is crucial in examining the efficiency of adaptive methods.

We first introduce the quantity of data oscillation

$$\operatorname{osc}(f,\mathcal{M}_H) := \left(\sum_{K\in\mathcal{M}_H} \| H_K a_K^{-1/2}(f - f_K) \|_{L^2(K)}^2 \right)^{1/2}, \tag{3.1}$$

where f_K stands for the mean value of f over K. For ease of reference, we now recall the refinement strategy in [14].

Morin–Nochetto–Siebert (MNS)-refinement strategy. Given two parameters $0 < \theta, \hat{\theta} < 1$.

1. Select a subset $\hat{\mathcal{B}}_H$ of sides in $\mathcal{B}_H$ such that
$$\left(\sum_{e\in\hat{\mathcal{B}}_H} \eta_e^2 \right)^{1/2} \geq \theta \left(\sum_{e\in\mathcal{B}_H} \eta_e^2 \right)^{1/2}.$$
2. Let $\hat{\mathcal{M}}_H$ be the set of elements with one side in $\hat{\mathcal{B}}_H$. Enlarge $\hat{\mathcal{M}}_H$ such that
$$\operatorname{osc}(f,\hat{\mathcal{M}}_H) \geq \hat{\theta}\operatorname{osc}(f,\mathcal{M}_H).$$
3. Refine every element in $\hat{\mathcal{M}}_H$ in such a way that a node is created in the interior of the element.

The convergence analysis starts from the orthogonality result which can be easily proved by the Galerkin orthogonality.

LEMMA 3.1. *If $\mathcal{M}_h$ is a local refinement of $\mathcal{M}_H$ such that $V^H \subset V^h$, the following relation holds:*

$$|\!|\!| u - u_h |\!|\!|_\Omega^2 = |\!|\!| u - u_H |\!|\!|_\Omega^2 - |\!|\!| u_h - u_H |\!|\!|_\Omega^2.$$

The following local bound for the error decrease plays the key role in the convergence analysis. The proof is similar to that of [14, Lemma 4.2] and thus is omitted.

LEMMA 3.2. *Let $\mathcal{M}_h$ be a refinement of $\mathcal{M}_H$ according to the MNS-refinement strategy. Then there exist constants $C_4, C_5 \geq 1$ depending only on the minimum angle of the mesh $\mathcal{M}_H$ such that for all $e \in \hat{\mathcal{B}}_H$ (the collection of all sides belonging to the marked elements) we have*

$$\eta_e^2 \leq C_4\Lambda_e \sum_{K\in\Omega_e} |\!|\!| u_h - u_H |\!|\!|_K^2 + C_5\Lambda_e \sum_{K\in\Omega_e} \| H_K a_K^{-1/2}(f - f_K) \|_{L^2(K)}^2. \tag{3.2}$$

Here we recall that $\Lambda_e = \max_{K\in\Omega_e}(\Lambda_K)$.

The presence of the factor Λ_e in the local lower bound measuring the error decrease in (3.2) is crucial in affecting the error reduction rate and thus the overall behavior of the adaptive method. In the appendix of the paper we will construct a counterexample to show this factor in general *cannot* be removed. Again we remark that Λ_e is equal to one on sides away from the singular nodes.

Now let $\Lambda = \max_{K\in\mathcal{M}_H}(\Lambda_K)$, and summing up in $e \in \hat{\mathcal{B}}_H$ in (3.2) we get

$$\sum_{e\in\hat{\mathcal{B}}_H} \eta_e^2 \le 2C_4\Lambda |\!|\!| u_h - u_H |\!|\!|_\Omega^2 + 2C_5\Lambda \mathrm{osc}(f,\mathcal{M}_H)^2.$$

Hence, from step 1 in the MNS-refinement strategy and Theorem 2.1, we obtain

$$|\!|\!| u - u_H |\!|\!|_\Omega^2 \le C_1 \sum_{e\in\mathcal{B}_H} \eta_e^2 \le C_1\theta^{-2}\Big(2C_4\Lambda |\!|\!| u_h - u_H |\!|\!|_\Omega^2 + 2C_5\Lambda \mathrm{osc}(f,\mathcal{M}_H)^2\Big),$$

which yields

$$|\!|\!| u_h - u_H |\!|\!|_\Omega^2 \ge \frac{\theta^2}{2C_1C_4\Lambda} |\!|\!| u - u_H |\!|\!|_\Omega^2 - \frac{C_5}{C_4}\mathrm{osc}(f,\mathcal{M}_H)^2.$$

Consequently, in view of Lemma 3.1,

$$|\!|\!| u - u_h |\!|\!|_\Omega^2 \le \alpha^2 |\!|\!| u - u_H |\!|\!|_\Omega^2 + \frac{C_5}{C_4}\mathrm{osc}(f,\mathcal{M}_H)^2, \quad \alpha = \left(1 - \frac{\theta^2}{2C_1C_4\Lambda}\right)^{1/2}. \tag{3.3}$$

The proof of the following lemma is similar to that of [14, Corollary 4.3] and thus is omitted.

LEMMA 3.3. *Let $\gamma \in (0,1)$ be the reduction factor of element size associated with one refinement step. Given $\hat{\theta} \in (0,1)$, let $\hat{\alpha} = (1-(1-\gamma^2)\hat{\theta}^2)^{1/2}$. Let $\mathcal{M}_h$ be a refinement of $\mathcal{M}_H$ according to the MNS-refinement strategy; then we have*

$$\mathrm{osc}(f,\mathcal{M}_h) \le \hat{\alpha}\mathrm{osc}(f,\mathcal{M}_H). \tag{3.4}$$

Based on this lemma and property (3.3), we have the following error reduction property.

THEOREM 3.4. *Let $\beta \in \mathbf{R}$ satisfy $\max(\alpha,\hat{\alpha}) < \beta < 1$, and let*

$$C_0 = \left(|\!|\!| u - u_0 |\!|\!|_\Omega^2 + \frac{C_5}{C_4(\beta^2 - \min(\alpha,\hat{\alpha})^2)}\mathrm{osc}(f,\mathcal{M}_0)^2\right)^{1/2}.$$

Then the adaptive algorithm based on the MNS-refinement strategy using the local a posteriori error indicator (2.4) produces a convergent sequence $\{u_k\}_{k\ge1}$ of discrete solutions such that $|\!|\!| u - u_k |\!|\!|_\Omega \le C_0\beta^k$.

Proof. The following proof is different from that of [14] and is more straightforward. Let $a_k = |\!|\!| u - u_k |\!|\!|_\Omega^2$ and $b_k = \frac{C_5}{C_4}\mathrm{osc}(f,\mathcal{M}_k)^2$. Then from (3.3) and (3.4) we know that

$$a_{k+1} \le \alpha^2 a_k + b_k, \quad b_k \le \hat{\alpha}^2 b_{k-1}. \tag{3.5}$$

By repeatedly using the left inequality in (3.5) we get

$$\begin{aligned} a_{k+1} &\le \alpha^2(\alpha^2 a_{k-1} + b_{k-1}) + b_k \\ &= \alpha^{2\cdot 2} a_{k-1} + \alpha^2 b_{k-1} + b_k \\ &\le \cdots\cdots \\ &\le \alpha^{2(k+1)} a_0 + \sum_{j=0}^{k} \alpha^{2j} b_{k-j}. \end{aligned}$$

On the other hand, we deduce from the right inequality in (3.5) that $b_{k-j} \le \hat{\alpha}^{2(k-j)} b_0$ for any $0 \le j \le k$. Thus

$$\begin{aligned} a_{k+1} &\le \beta^{2(k+1)} a_0 + \sum_{j=0}^{k} \alpha^{2j} \hat{\alpha}^{2(k-j)} b_0 \\ &\le \beta^{2(k+1)} a_0 + \beta^{2k} b_0 \cdot \sum_{j=0}^{k} \left(\frac{\rho}{\beta}\right)^{2j} \\ &\le \beta^{2(k+1)} a_0 + \beta^{2k} b_0 \cdot \frac{1}{1-\rho^2/\beta^2} \\ &\le \beta^{2(k+1)} \left(a_0 + \frac{b_0}{\beta^2 - \rho^2}\right), \end{aligned}$$

where $\rho = \min(\alpha, \hat{\alpha})$. This completes the proof. ∎

To conclude this section, we give a few remarks.

Remark 3.1. The reduction rate β depends on two constants $\alpha, \hat{\alpha}$. Usually $\gamma \le 1/2$; from Lemma 3.3 we know that $\hat{\alpha} \le 0.8$ if $\hat{\theta} = 2\sqrt{3}/5 \approx 0.6928$. This is rather satisfactory in most of the practical problems involving strong singularities. The choice of the parameter $\hat{\theta}$ is discussed in [14]. We will study the effect of the parameter θ in the next section through numerical experiments.

Remark 3.2. The dependence of the error reduction β on the product of the upper bound and lower bound constants C_1, C_4 is quite revealing. It indicates that the precise information of the upper bound constant C_1 is not of much importance in the adaptive procedures based on the a posteriori error estimates. It is the inherent structure of the a posteriori error indicators that determines the performance of the adaptive algorithm.

Remark 3.3. For the error estimator (1.6), the following local lower bound similar to that of (3.2) holds:

$$\hat{\eta}_e^2 \le \hat{C}_4 \sum_{K \in \Omega_e} |\!|\!| u_h - u_H |\!|\!|_K^2 + \hat{C}_5 \sum_{K \in \Omega_e} \| H_K a_K^{-1/2} (f - f_K) \|_{L^2(K)}^2,$$

where $\hat{\eta}_e^2 = \sum_{K \in \Omega_e} \| H_K a_K^{-1/2} f \|_{L^2(K)}^2 + \| H_e^{1/2} a_e^{-1/2} J_e \|_{L^2(e)}^2$, and $\hat{C}_4, \hat{C}_5$ are positive constants depending only on the minimum angle of the mesh $\mathcal{M}_H$. If the mesh $\mathcal{M}_H$ has singular nodes, then the upper bound (1.5) becomes

$$|\!|\!| u - u_H |\!|\!|_\Omega^2 \le \hat{C}_1 \Lambda \sum_{e \in \mathcal{B}_H} \hat{\eta}_e^2,$$

where the constant $\hat{C}_1$ depends only on the minimum angle of the mesh $\mathcal{M}_H$. Let $\{\hat{u}_k\}_{k \ge 1}$ be the sequence generated by the adaptive algorithm based on the MNS-refinement strategy using the local a posteriori error indicator (1.6). Then from Theorem 3.4 we expect that the convergence rate of $|\!|\!| \hat{u}_k - u |\!|\!|_\Omega$ will be similar to that of $|\!|\!| u_k - u |\!|\!|_\Omega$. This is indeed observed in our numerical experiments shown in section 4.1. However, since our error estimator emphasizes the contribution of the local error estimators from the singular nodes, it does have advantages in resolving the singularities as can be seen from our numerical results in section 4.1.

Remark 3.4. The appearance of the quantity Λ in the definition of α indicates that the error reduction rate β will get close to 1 as the jump of coefficient gets large.

This fact is also observed in our numerical experiments in section 4.3. This interesting point reflects the essence or limitation of the adaptive methods. The adaptive methods under investigation provide an efficient way to find the discrete solution with error control. However, the singular nature of the original problems remains unchanged and indeed is reflected in the performance of the algorithm.

4. Numerical experiments. In this section we first show some of our extensive numerical experiments to further explain the performance of our new error indicator in section 2 and the influence of the parameter θ to the efficiency of the adaptive method. We also report some numerical experiments to demonstrate the error reduction rate β is indeed dependent on the jump of the coefficients. This supports our theoretical result in Theorem 3.4 and the argument in Remark 3.4.

We choose the numerical example used in [14, section 5.3] to run our experiments. An exact solution of the elliptic problem with piecewise constant coefficients and vanishing right-hand side f is constructed by using the formulas derived by Kellogg [12]. Let $\Omega = (-1,1)^2$, $a(x) = R$ in the first and third quadrants and $a(x) = 1$ in the second and fourth quadrants. An exact weak solution u of (1.1) for $f = 0$ is given in polar coordinates by $u(r,\vartheta) = r^\gamma \mu(\vartheta)$, where

$$\mu(\vartheta) = \begin{cases} \cos((\pi/2-\sigma)\gamma)\cdot\cos((\vartheta-\pi/2+\rho)\gamma) & \text{if} \quad 0 \le \vartheta \le \pi/2, \\ \cos(\rho\gamma)\cdot\cos((\vartheta-\pi+\sigma)\gamma) & \text{if} \quad \pi/2 \le \vartheta \le \pi, \\ \cos(\sigma\gamma)\cdot\cos((\vartheta-\pi-\rho)\gamma) & \text{if} \quad \pi \le \vartheta \le 3\pi/2, \\ \cos((\pi/2-\rho)\gamma)\cdot\cos((\vartheta-3\pi/2-\sigma)\gamma) & \text{if} \quad 3\pi/2 \le \vartheta \le 2\pi \end{cases}$$

and the numbers γ, ρ, σ, R satisfy the nonlinear relations

$$\begin{cases} R = -\tan((\pi/2-\sigma)\gamma)\cdot\cot(\rho\gamma), \\ 1/R = -\tan(\rho\gamma)\cdot\cot(\sigma\gamma), \\ R = -\tan(\sigma\gamma)\cdot\cot((\pi/2-\rho)\gamma), \\ 0 < \gamma < 2, \\ \max(0, \pi\gamma - \pi) < 2\gamma\rho < \min(\pi\gamma, \pi), \\ \max(0, \pi - \pi\gamma) < -2\gamma\sigma < \min(\pi, 2\pi - \pi\gamma). \end{cases} \tag{4.1}$$

This solution u is in Sobolev space $H^{1+\delta}(\Omega)$ with $\delta < \gamma$ and thus is very singular for small parameter γ. For example, when $\gamma = 0.1$, (4.1) is solved in [14] to obtain

$$R \approx 161.4476387975881, \quad \rho = \pi/4, \quad \sigma \approx -14.92256510455152. \tag{4.2}$$

The surface plot of the resultant solution u is depicted in Figure 1. Let u_n be the finite element approximation of u on a uniform mesh constructed by first dividing the domain into $n \times n$ subdomains and then connecting the lower left and upper right corners of each subdomain. The surface plot of the relative error $(u - u_{1024})/\| u \|_{L^\infty(\Omega)}$ is depicted in Figure 2. The relative error is about 23.68 percent around the singularity point. The energy error $\|\!| u - u_{1024} |\!|_\Omega$ is 0.6954, a very slow decrease from $\|\!| u - u_{128} |\!|_\Omega = 0.8547$. Since the solution u is in Sobolev space $H^{1+\delta}(\Omega)(\delta < 0.1)$, we know from standard finite element a priori error analysis that to bring the energy error below 0.1, we must introduce 10^{11} nodes in each space direction. Therefore, the standard

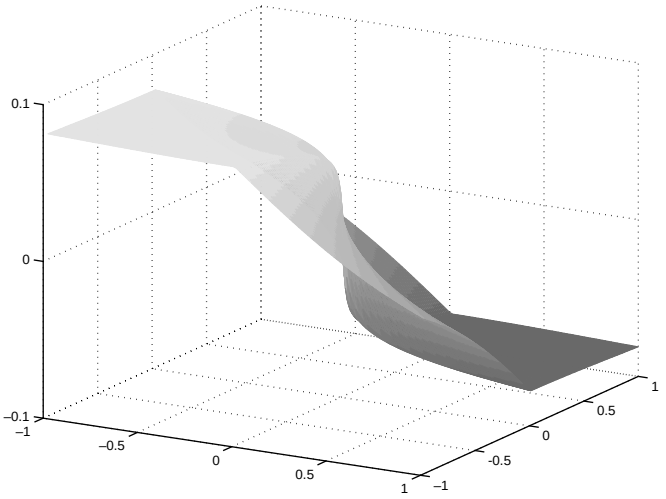

FIG. 1. *The surface plot of the exact solution u for $\gamma = 0.1$.*

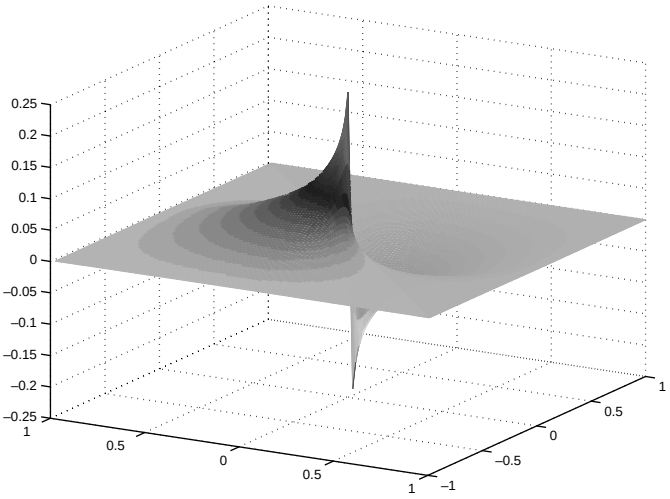

FIG. 2. *The surface plot of the relative error $(u - u_{1024})/\| u \|_{L^\infty(\Omega)}$. The maximum of the relative error is* 0.2368.

finite element method with uniform mesh is not appropriate for solving such elliptic problems with strong singularities. However, our adaptive method requires only 2793 nodes to achieve an energy error of 0.07303. The surface plot of the relative error $(u - u_h)/\| u \|_{L^\infty(\Omega)}$ is depicted in Figure 3. The maximum of the relative error is 0.011719, less than 2 percent around the singularity point.

4.1. Influence of error estimators. We compare the performance of our new local error indicator proposed in this paper with the performance of the estimators (1.3), (1.6). The computations are carried out on a SUN Ultra 10 workstation. In the implementation of the adaptive algorithm (1.9), we use the MNS-refinement strategy in section 3. We use the method indicated in Figure 4 to refine a marked element which creates an interior node.

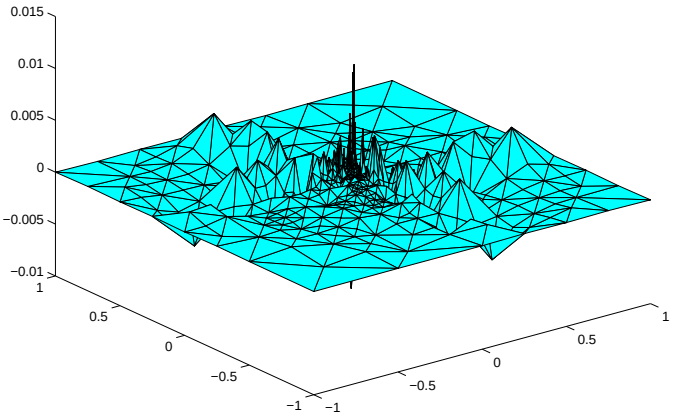

FIG. 3. *The surface plot of the relative error* $(u - u_h)/\| u \|_{L^\infty(\Omega)}$ *of the adaptive solution* u_h *on an adaptive mesh of* 2793 *nodes. The maximum of the relative error is* 0.011719.

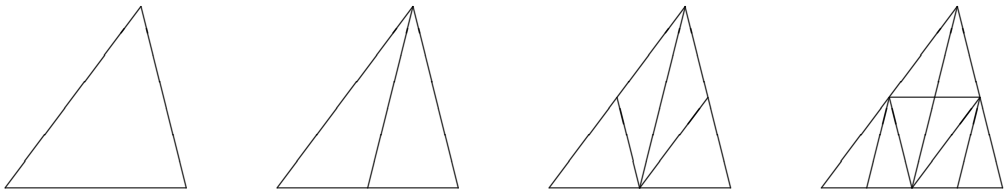

FIG. 4. *Refinement of a marked triangle which generates an interior node.*

In this subsection, we take $\gamma = 0.1$ and the parameters R, ρ, σ according to (4.2) to define the exact solution that we are going to approximate. This exact solution is displayed in Figure 1. Since the source $f = 0$, we need not specify the parameter $\hat{\theta}$ in the MNS-refinement strategy. We take the parameter $\theta = 0.2$ which seems to perform best, as will be seen in section 4.2. In what follows, we refer to the adaptive algorithm using the estimators (1.3), (1.6), and (1.8) as the Babuška–Miller (BM), Bernardi–Verfürth (BV), and NEW methods, respectively.

Denote by $I_h u$ the linear interpolant of the exact solution on the mesh $\mathcal{M}_h$. In the computations, we are interested in the norm $\| I_h u - u_h \|_{L^\infty(\Omega)}$ which measures the error between u_h and u on the nodes. We are also interested in the energy error $\|\!| u - u_h |\!|\!|_\Omega$ which is computed through the following formula which can be easily proved by simple integration by parts [15]:

$$|\!| u - u_h |\!|\!|_\Omega^2 = \int_\Omega f(u - 2u_h)dx + \int_{\partial\Omega} (a(x)\nabla u \cdot \nu)(u - 2u_h)ds + |\!| u_h |\!|\!|_\Omega^2.$$

Note that in our example, $f = 0$ and the solution u is smooth on the boundary, so standard numerical quadrature will provide rather accurate approximations. Our numerical experiments show that both the BV and the NEW methods perform better than the BM method. The NEW method converges faster than the BV method in terms of $\| I_h u - u_h \|_{L^\infty(\Omega)}$. That is, the NEW method provides better nodal value approximations than the BV method due to the magnification of the local error

TABLE 1
The iteration number k, the number of nodes n, the CPU time, and the errors when $\| I_h u - u_h \|_{L^\infty(\Omega)} \leq 0.001$.

	k	n	CPU time	$\| I_h u - u_h \|_{L^\infty(\Omega)}$	$\|\!\| u - u_h \|\!\|_\Omega$
BM	56	4606	160.0s	0.9560E-03	0.6750E-01
BV	54	7039	445.0s	0.9760E-03	0.3915E-01
NEW	59	1538	70.0s	0.9902E-03	0.1037E-00

TABLE 2
The iteration number k, the number of nodes n, the CPU time, and the errors when the number of nodes of different methods is roughly 50000.

	k	n	CPU time	$\| I_h u - u_h \|_{L^\infty(\Omega)}$	$\|\!\| u - u_h \|\!\|_\Omega$
BM	83	50389	6711.0s	0.2704E-03	0.2607E-01
BV	75	51893	11429.0s	0.1451E-03	0.1427E-01
NEW	111	52112	12173.0s	0.4643E-04	0.1427E-01

estimators around the singular nodes in the NEW method. On the other hand, the performance of both the BV and NEW method is comparable in terms of the energy error $|\!|\!| u - u_h |\!|\!|_\Omega$.

In Table 1, we show the iteration number, the number of nodes, the CPU time, and the final errors for different methods when $\| I_h u - u_h \|_{L^\infty(\Omega)}$ less than 0.001. The corresponding final finite element meshes are displayed in Figure 5.

In Table 2, we show the iteration number, the number of nodes, the CPU time, and the final errors for different methods when the number of nodes of each method is over 50000. The corresponding final finite element meshes are displayed in Figure 6.

From Figure 7 we observe that all three methods perform similarly for the coarse grids (when $\mathrm{DOFs}(k) \leq 1000$). Moreover, for all three methods, the meshes and the associated numerical complexity are quasi-optimal [14]: $|\!|\!| u - u_k |\!|\!|_\Omega = C\ \mathrm{DOFs}(k)^{-1/2}$ is valid asymptotically. (The performance of the quasi-optimal method is indicated by the straight line of slope $-1/2$.) For the same amount of nodes used, the performances of the BV and NEW methods are comparable, but all are better than the BM method. Figure 8 is quite interesting. It demonstrates that the NEW method provides better nodal value approximation to the true solution than the BV and BM methods do. This may be explained as the NEW method tends to put more nodes around the singular point where the error is the largest. Moreover, the meshes and the associated numerical complexity are also quasi-optimal in terms of the nodal value approximation for the BV and NEW methods: $\| I_k u - u_k \|_{L^\infty(\Omega)} = C\ \mathrm{DOFs}(k)^{-1}$ is valid asymptotically. (The performance of the quasi-optimal method is indicated by the straight line of slope -1.)

4.2. Influence of the parameter θ. In this subsection, we examine the influence of the parameter θ in MNS-refinement strategy on the performance of the adaptive algorithm based on our new local error estimator. We take $\gamma = 0.1$ and the parameters R, ρ, σ according to (4.2) to define the exact solution that we are going to approximate.

Table 3 reports the iteration number, the number of nodes of the final meshes, the CPU time, and the final errors for different choices of the parameter θ. The stopping

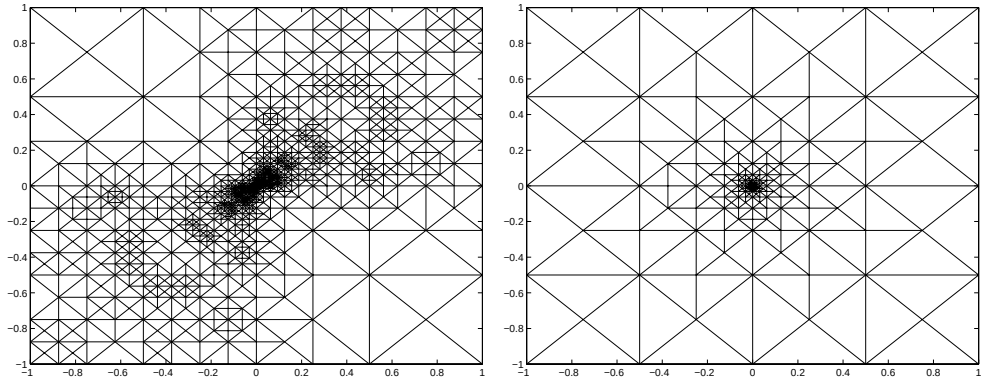

FIG. 5. *The mesh of* 4606 *nodes generated by the BM method (left) and the mesh of* 1538 *nodes generated by the NEW method (right). The error* $\| I_h u - u_h \|_{L^\infty(\Omega)}$ *of the finite element solutions on both meshes are roughly the same.*

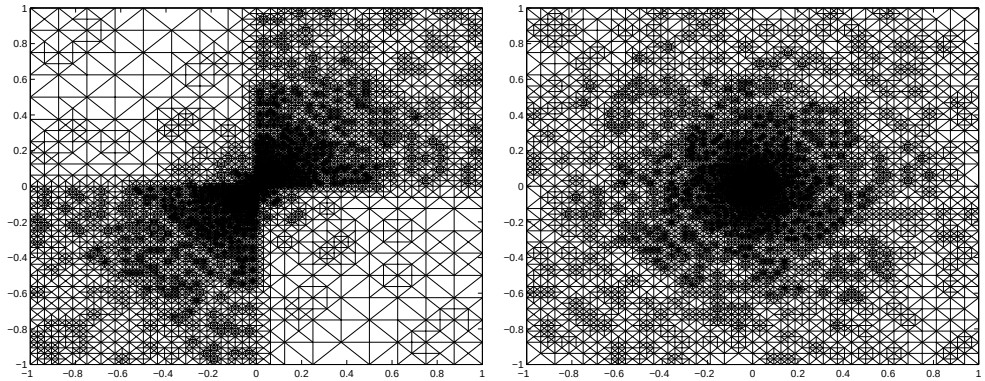

FIG. 6. *The mesh of* 50389 *nodes generated by the BM method (left) and the mesh of* 52112 *nodes generated by using the NEW method (right). The energy error of the finite element solution on the right mesh is much less (*55 *percent) of the one on the left mesh.*

criterion is taken as the reduction rate $\eta_k/\eta_0 \leq 0.01$ or the number of degrees of freedom DOFs ≥ 50000.

In Figure 9 we show the number of degrees of freedom at each iteration. In Figure 10 we demonstrate the performance of the adaptive algorithm under different choices of the parameter θ.

Clearly, from every point of view, the choice $\theta = 0.5$ is the worst. This is not surprising, since a large θ may cause unnecessary refinements at those nonsingular domains. And this is also the reason why there is an abrupt increase in the number of degrees of freedom for $\theta = 0.5$. The choice $\theta = 0.3$ also contains an abrupt jump in the number of nodes. The results for $\theta = 0.3$ are better than the choice of $\theta = 0.5$ but worse than the other two choices of $\theta = 0.1, 0.2$.

The choice $\theta = 0.1$ is slightly better than that of $\theta = 0.2$ in terms of the degrees of freedom. However, it uses many more steps and much more CPU time. Overall, the choice of $\theta = 0.2$ performs best.

We conclude from the above observations that the choice of the parameter θ can greatly affect the overall behavior of the adaptive algorithm. In practical applications,

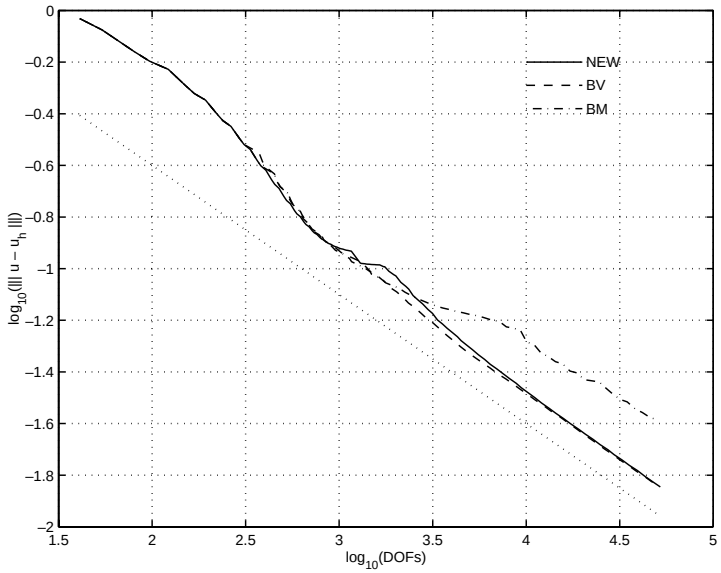

FIG. 7. *Quasi optimality of the estimators. The quasi-optimal decay is indicated by the dotted line of slope* $-1/2$.

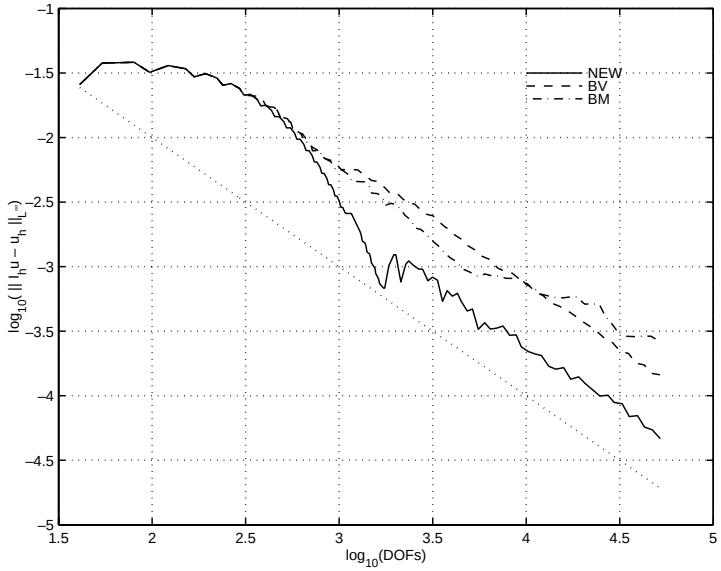

FIG. 8. *Performance of the estimators in terms of the nodal value approximations. The quasi-optimal decay is indicated by the dotted line of slope* -1.

one may use a variable parameter θ: larger θ at the initial iterations and smaller ones after a certain number of iterations.

We also remark that there is a big difference between the iterations of the adaptive finite element methods and the iterations in other iterative methods such as Gauss–Seidel or conjugate gradient methods for solving linear system of equations. For the Gauss–Seidel or conjugate gradient methods for solving linear system of equations, the

TABLE 3

The iteration number k, the number of nodes n, the CPU time, and the errors for different choices of θ.

θ	k	n	CPU time	$\| I_h u - u_h \|_{L^\infty(\Omega)}$	$\|\!\|\!\| u - u_h \|\!\|\!\|_\Omega$	η_k/η_0
0.1	153	8094	2167.0s	0.2820E-03	0.3750E-01	0.9972E-02
0.2	90	8151	713.0s	0.2937E-03	0.3750E-01	0.9988E-02
0.3	70	187311	17232.0s	0.8252E-03	0.4486E-01	0.1200E-01
0.5	55	173136	13086.0s	0.2017E-02	0.6378E-01	0.1776E-01

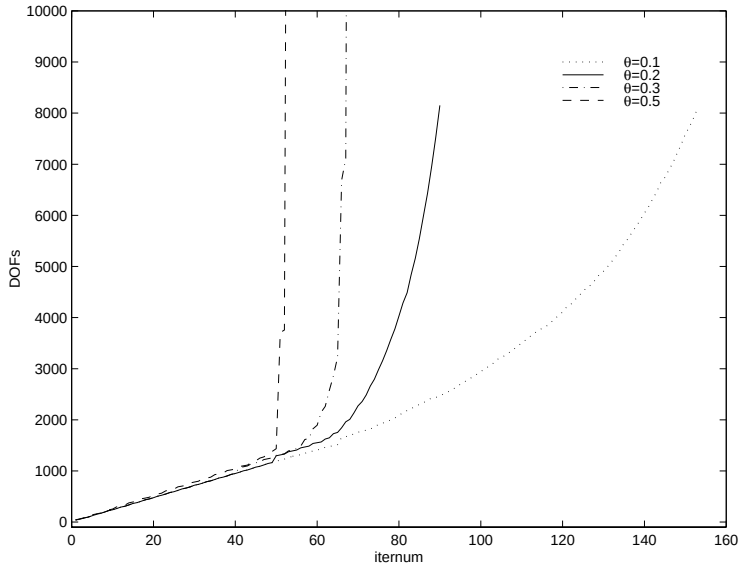

FIG. 9. *Comparison of the degrees of freedom at each iteration for $\theta = 0.1, 0.2, 0.3, 0.5$.*

computational complexity is the same at each iteration. In this case, it is important to consider the convergence rate which determines the number of iterations and thus the overall computational cost. On the other hand, the computational complexity is different in different iteration steps in the adaptive finite element methods. It is the last several steps of the adaptive iteration that use most of the CPU time. In this case, it may happen that theoretically the rate of convergence is faster in some cases; e.g., different values of θ may cause different values of β, and a larger θ may get a smaller β, but in practice the situation may be worse due to the abrupt increase of computational complexity.

4.3. Influence of the singularities. In this subsection we show that the error reduction rate β gets close to 1 when the singularity of the problem gets stronger. This confirms the theoretical results in section 3. In the computations we take the parameter $\theta = 0.2$. We will compare three kinds of singularities which correspond to choosing $\gamma = 0.02, 0.1, 0.5$ in the example stated at the beginning of this section. For $\gamma = 0.02$, the parameters R, ρ, σ are given by

$$R \approx 4052.1806954768103, \quad \rho = \pi/4, \quad \sigma \approx -77.754418176347386. \tag{4.3}$$

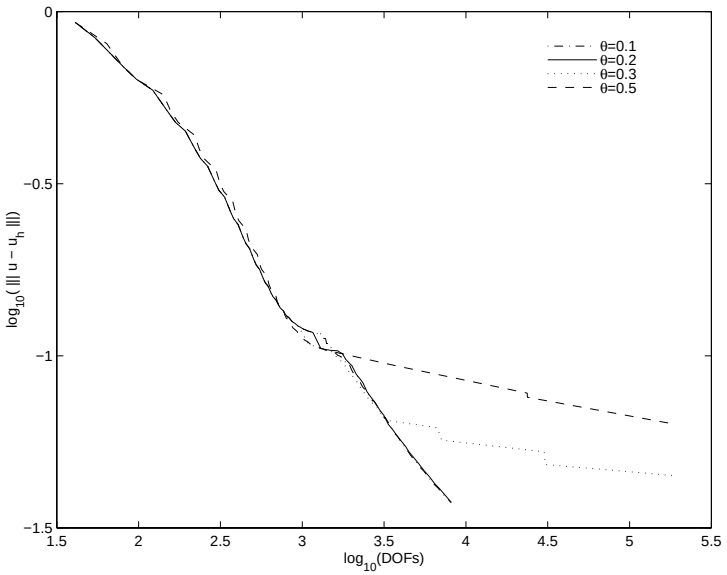

FIG. 10. *Comparison of the performance for* $\theta = 0.1, 0.2, 0.3, 0.5$.

TABLE 4

The iteration number k*, the number of nodes* n*, the CPU time, and the errors for different choices of* γ*.*

γ	k	n	CPU time	$\| I_h u - u_h \|_{L^\infty(\Omega)}$	$\|\!\|\!\| u - u_h \|\!\|\!\|_\Omega$	η_k/η_0
0.02	202	4783	3215.0s	0.9094E-03	0.5993E-01	0.7268E-02
0.1	79	3778	226.0s	0.6511E-03	0.5876E-01	0.1557E-01
0.5	25	941	5.0s	0.1209E-02	0.5698E-01	0.1150E-00

For $\gamma = 0.5$, the parameters R, ρ, σ are given by

$$R \approx 5.8284271247461907, \quad \rho = \pi/4, \quad \sigma \approx -2.3561944901923448. \tag{4.4}$$

Table 4 shows the iteration number, the number of nodes of the final meshes, the CPU time, and the final errors when the energy errors are less than 0.06. Figure 11 depicts the final mesh of 4783 nodes for $\gamma = 0.02$ and the final mesh of 941 nodes for $\gamma = 0.5$. Figure 12 shows the perfomance of the adaptive algorithm based on the new estimator for different choices of singularities. We observe that the iteration number increases when the jump of the coefficients gets larger. This conforms with our theoretical result that the error reduction rate β is increasing as the jump of coefficients is increasing.

Let $\mathcal{E}_k = \sum_{e \in \mathcal{B}_k} \eta_e^2$ be the total estimated error at the kth iteration of the adaptive method using the a posteriori estimator proposed in the paper. Figure 13 shows the effective indices $\mathcal{E}_k / \|\!\|\!\| u - u_k \|\!\|\!\|_\Omega$ for different choices of $\gamma = 0.02, 0.1, 0.5$. Clearly our error estimator does not underestimate the error introduced by the pollution effects of strong singularities. Figure 14 is rather interesting. It shows that in the case of the weakly discontinuous coefficient $\gamma = 0.5$, our new estimator as well as the BV estimator behave like the usual BM estimator, as expected.

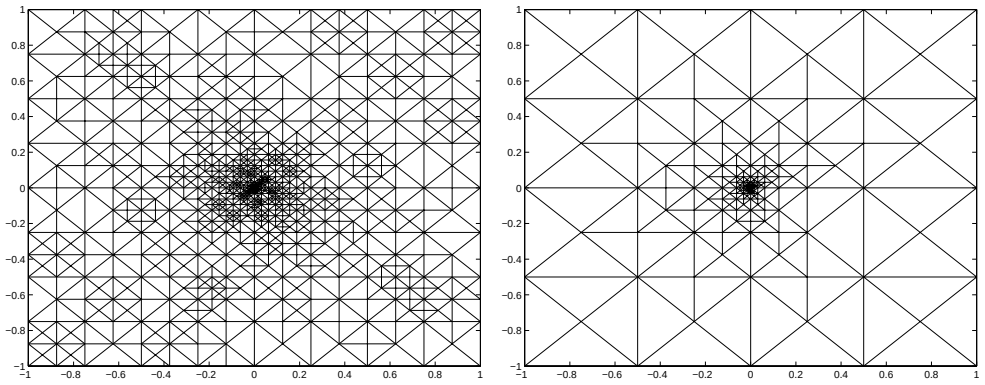

FIG. 11. *The mesh of* 4783 *nodes generated for* $\gamma = 0.02$ *(left) and the mesh of* 941 *nodes generated for* $\gamma = 0.5$ *(right).*

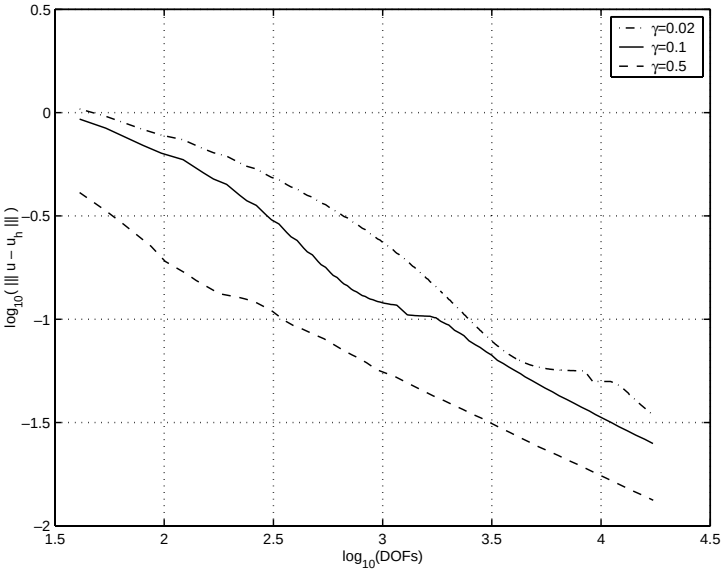

FIG. 12. *Comparison of the performance for* $\gamma = 0.02, 0.1, 0.5$.

5. Appendix. In this appendix we construct a counterexample to show that the factor Λ_e in the local lower bound in Lemma 3.2 cannot be removed. We consider the problem (1.1)–(1.2) on the domain $\Omega = (0,2) \times (0,2)$. The domain is divided into two parts by connecting the lower left and upper right corners as given in Figure 15. The coefficient $a(x)$ and the source $f(x)$ is given as follows:

$$a(x) = \begin{cases} 1 & \text{if } x \in \Omega_1, \\ R > 1 & \text{if } x \in \Omega_2, \end{cases} \qquad f(x) = \begin{cases} 0 & \text{if } x \in \Omega_1, \\ 1 & \text{if } x \in \Omega_2. \end{cases}$$

The coarse mesh $\mathcal{M}_H$ is shown in the middle of Figure 15 which has only one interior node denoted by 1 in the figure. The discrete solution $u_H \in V_0^H$ satisfies

$$(a\nabla u_H, \nabla v_H) = (f, v_H) \quad \forall v_H \in V_0^H.$$

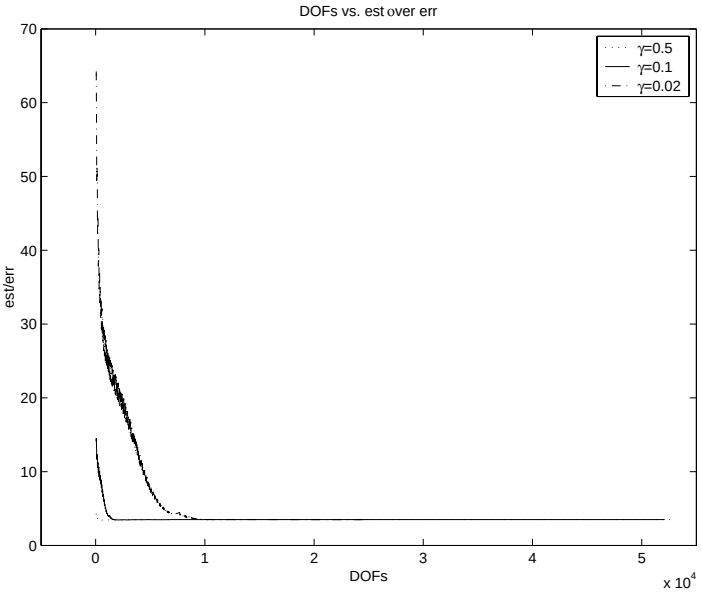

FIG. 13. *The effective indices for different choices of* $\gamma = 0.02, 0.1, 0.5$.

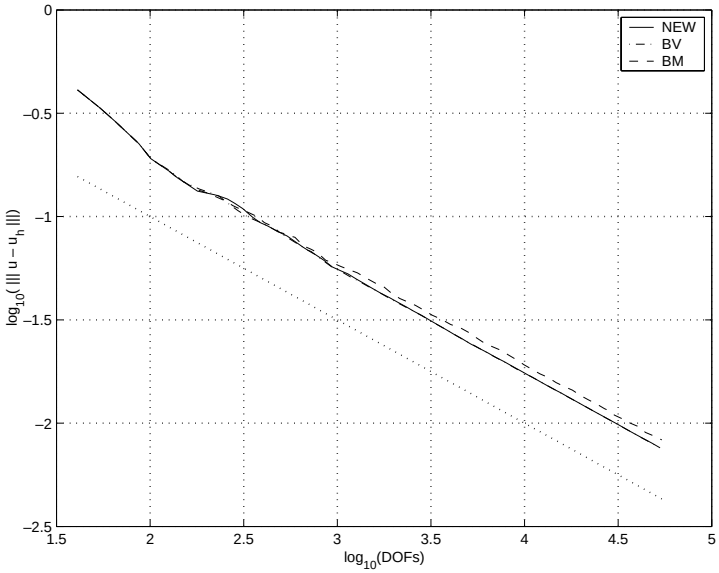

FIG. 14. *Quasi optimality of three methods when* $\gamma = 0.5$. *The quasi-optimal decay is indicated by the dotted line of slope* $-1/2$.

Let ψ_1^H be the linear nodal basis function of V_0^H corresponding to the node 1. Then simple calculations yield $u_H(x) = u_1^H \psi_1^H(x)$ with u_1^H satisfying the linear equation

$$(2 + 2R)u_1^H = \frac{1}{2}.$$

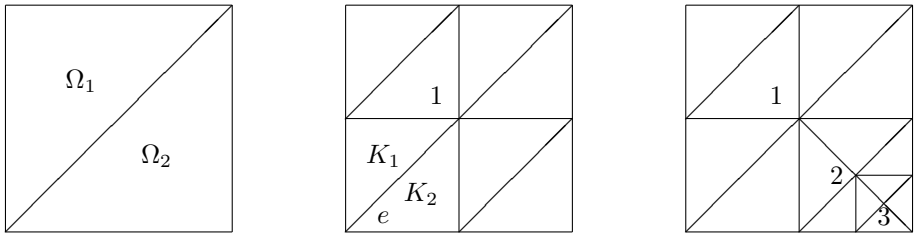

FIG. 15. *The domain Ω (left), the coarse mesh $\mathcal{M}_H$ (middle), and the fine mesh $\mathcal{M}_h$ (right).*

Thus $u_1^H = 1/(4+4R)$. Now consider the interior side e which is the common side of two elements K_1, K_2 as shown in Figure 15. Then $H_{K_1} = H_{K_2} = H_e = \sqrt{2}$, $|K_1| = |K_2| = 1/2$, $\Lambda_{K_1} = 1, \Lambda_{K_2} = R$, $\Lambda_e = R$, and $J_e = [\![a(x)\nabla u_H \cdot \nu]\!]|_e = (1+R)u_1^H/\sqrt{2} = 1/(4\sqrt{2})$. Thus the local error indicator η_e is

$$\eta_e^2 = \sum_{K\in\Omega_e} \Lambda_K \| H_K a_K^{-1/2} f \|_{L^2(K)}^2 + \Lambda_e \| H_e^{1/2} a_e^{-1/2} J_e \|_{L^2(e)}^2$$

$$= 1 + \frac{1}{16} = \frac{17}{16}. \tag{5.1}$$

Assume that the triangle in the lower right corner of the mesh $\mathcal{M}_H$ is marked for refinement which leads to a new refined mesh $\mathcal{M}_h$ as shown in Figure 15. Now there are three interior nodes labeled as 1, 2, and 3 as in the figure. The corresponding finite element basis functions are denoted by $\psi_j^h, j = 1, 2, 3$. The discrete solution $u_h \in V_0^h$ satisfies the discrete equation

$$(a\nabla u_h, \nabla v_h) = (f, v_h) \quad \forall v_h \in V_0^h.$$

Simple algebraic calculations yield that $u_h(x) = \sum_{j=1}^3 u_j^h \psi_j^h(x)$ with u_j^h the solution of the following linear system of equations:

$$\begin{pmatrix} 2+2R & -R & 0 \\ -R & 4R & -R \\ 0 & -R & 4R \end{pmatrix} \begin{pmatrix} u_1^h \\ u_2^h \\ u_3^h \end{pmatrix} = \begin{pmatrix} \frac{1}{2} \\ \frac{7}{24} \\ \frac{1}{12} \end{pmatrix}.$$

We have

$$u_1^h = \frac{35}{8(15+13R)}, \quad u_2^h = \frac{9R+5}{4R(15+13R)}, \quad u_3^h = \frac{20R+15}{24R(15+13R)}.$$

Note that the second term on the right-hand side of (3.2) vanishes. We need only to compute the energy error between u_h and u_H. Since $\psi_1^h = \psi_1^H$ and $\psi_2^h = \psi_3^h = 0$ in K_1, K_2, we get

$$\sum_{K\in\Omega_e} |\!|\!| u_h - u_H |\!|\!|_K^2 = \int_{K_1\cup K_2} a(x)|\nabla(u_h - u_H)|^2 dx$$

$$= \int_{K_1\cup K_2} a(x)|u_1^h - u_1^H|^2 |\nabla\psi_1^H|^2 dx$$

$$= |u_1^h - u_1^H|^2 \cdot \frac{1}{2}(1+R)$$

$$= \frac{(9R+5)^2}{128(1+R)(15+13R)^2}.$$

This, together with (5.1) and $\Lambda_e = R$, yields

$$\lim_{R\to\infty} \frac{\eta_e^2}{\Lambda_e \sum_{K\in\Omega_e} \|u_h - u_H\|_K^2} = \frac{22984}{81}.$$

This indicates that the factor Λ_e in the local lower bound (3.2) is sharp and cannot be removed.

Acknowledgment. The authors would like to thank the anonymous referees for their helpful comments which greatly improved the paper.

REFERENCES

[1] K. Aziz and A. Settari, *Petroleum Reservoir Simulations,* Applied Science Publishers, New York, 1979.

[2] I. Babuška and A. Miller, *A feedback finite element method with a posteriori error estimation: Part* I. *The finite element method and some basic properties of the a posteriori error estimator,* Comput. Meth. Appl. Mech. Engrg., 61 (1987), pp. 1–40.

[3] I. Babuška and W. C. Rheinboldt, *Error estimates for adaptive finite element computations,* SIAM J. Numer. Anal., 15 (1978), pp. 736–754.

[4] C. Bernardi and R. Verfürth, *Adaptive finite element methods for elliptic equations with non-smooth coefficients,* Numer. Math., 85 (2000), pp. 579–608.

[5] Z. Chen and S. Dai, *Adaptive Galerkin methods with error control for a dynamical Ginzburg–Landau model in superconductivity,* SIAM J. Numer. Anal., 38 (2001), pp. 1961–1985.

[6] Z. Chen and R.H. Nochetto, *Residual type a posteriori estimates for elliptic obstacle problems,* Numer. Math., 84 (2000), pp. 527–548.

[7] Z. Chen, R.H. Nochetto, and A. Schmidt, *A characteristic Galerkin method with adaptive error control for continuous casting problem,* Comput. Methods Appl. Mech. Engrg., 189 (2000), pp. 249–276.

[8] S. Dai, *Adaptive Finite Element Methods for Elliptic Problems with Strongly Discontinuous Coefficients,* Master's degree thesis, Institute of Computational Mathematics, Chinese Academy of Sciences, Beijing, China, 2000 (in Chinese).

[9] W. Dörfler, *A convergent adaptive algorithm for Poisson's equation*, SIAM J. Numer. Anal., 33 (1996), pp. 1106–1124.

[10] M. Dryja, M.V. Sarkis, and O.B. Widlund, *Multilevel Schwarz methods for elliptic problems with discontinuous coefficients in three dimensions,* Numer. Math., 72 (1996), pp. 313–348.

[11] K. Eriksson and C. Johnson, *Adaptive finite element methods for parabolic problems.* I: *A linear model problem*, SIAM J. Numer. Anal., 28 (1991), pp. 43–77.

[12] R.B. Kellogg, *On the Poisson equation with intersecting interface,* Appl. Anal., 4 (1975), pp. 101–129.

[13] R. Lewandowski, *Analyse mathématique et océanographie,* Collection Recherches en Mathématiques Appliquées, Masson, Paris, 1997.

[14] P. Morin, R.H. Nochetto, and K.G. Siebert, *Data oscillation and convergence of adaptive FEM,* SIAM J. Numer. Anal., 38 (2000), pp. 466–488.

[15] P. Morin, R.H. Nochetto, and K.G. Siebert, *Local problems on stars: A posteriori error estimators, convergence, and performance,* Math. Comp., to appear.

[16] R.H. Nochetto, A. Schmidt, and C. Verdi, *A posteriori error estimation and adaptivity for degenerate parabolic problems,* Math. Comp., 69 (2000), pp. 1–24.

[17] M. Petzoldt, *A Posteriori Error Estimators for Elliptic Equations with Discontinuous Diffusion Coefficients,* Preprint 533, WIAS Berlin, Berlin, Germany, 2000; also available online from http://www.wias-berlin.de/publications/preprints/533.

[18] M. Petzoldt,*Regularity Results for Interface Problems in* 2D, Preprint 565, WIAS Berlin, Berlin, Germany, 2000; also available online from http://www.wias-berlin.de/publications/preprints/565.

[19] R. Verfürth, *A Review of A Posteriori Error Estimation and Adaptive Mesh Refinement Techniques*, Teubner, Stuttgart, 1996.